ACS APPLIED MATERIALS & INTERFACES

RESEARCH ARTICLE

www.acsami.org

Enhanced Photoluminescence and Field-Emission Behavior of Vertically Well Aligned Arrays of In-Doped ZnO Nanowires

Mashkoor Ahmad,[†,‡] Hongyu Sun,[†] and Jing Zhu*[,†]

[†]Beijing National Center for Electron Microscopy, The state key Laboratory of New Ceramics and Fine Processing, Laboratory of Advanced Material, China Iron & Steel Research Institute Group, Department of Material Science and Engineering, Tsinghua University, Beijing 100084, China

[‡]Physics Division PINSTECH, Islamabad, Pakistan

ABSTRACT: Vertically oriented well-aligned Indium doped ZnO nanowires (NWs) have been successfully synthesized on Au-coated Zn substrate by controlled thermal evaporation. The effect of indium dopant on the optical and field-emission properties of these well-aligned ZnO NWs is investigated. The doped NWs are found to be single crystals grown along the *c*-axis. The composition of the doped NWs is confirmed by X-ray diffraction (XRD), energy-dispersive spectroscopy (EDS), and X-ray photospectroscopy (XPS). The photoluminescence (PL) spectra of doped NWs having a blue-shift in the UV region show a prominent tuning in the optical band gap, without any significant peak relating to intrinsic defects. The turn-on field of the field emission is found to be ~2.4 V μm^{-1} and an emission current density of 1.13 mA cm^{-2} under the field of 5.9 V μm^{-1}. The field enhancement factor β is estimated to be 9490 ± 2, which is much higher than that of any previous report. Furthermore, the doped NWs exhibit good emission current stability with a variation of less than 5% during a 200 s under a field of 5.9 V μm^{-1}. The superior field emission properties are attributed to the good alignment, high aspect ratio, and better crystallinity of In-doped NWs.

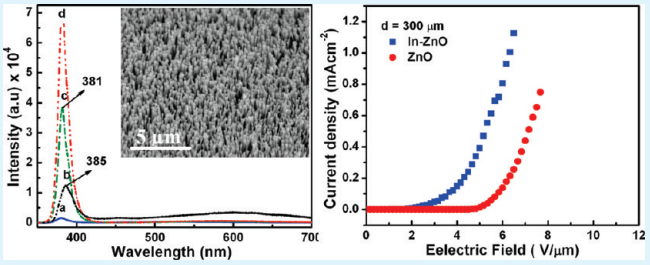

KEYWORDS: indium dopant, photoluminescence, field emission, enhancement factor

1. INTRODUCTION

High-quality field emitters are very desirable for applications in a wide range of field-emission (FE)-based devices such as flat-panel displays, vacuum microwave amplifiers, parallel-electron-beam microscopes, X-ray source, etc. One-dimensional 1D nanostructure are ideal candidates for achieving high field emission FE current density at a low electric field because of their high aspect ratio, low work function, and high mechanical stabilities and conductivities.[1−3] ZnO, with a direct band gap of E_g = 3.37 eV and a high exciton binding energy 60 meV, is considered one of the most promising semiconducting materials for blue or ultraviolet emission and its applications in optical and electrical industries, such as diodes and laser devices. In addition, it has also been found potentially useful in low-voltage FE devices,[4] becausee of its low electron affinity,[5] high thermal stability, as well as high oxidation resistance in harsh environments.

On the other hand, to develop efficient field emission devices based on ZnO nanostructures at a lowest energy expense, effective methods to improve their electron field-emission properties are highly desirable. Recently, sufficient efforts such as coated with amorphous carbon and carbon nitride films,[6] doping with selective elements,[7,8] ion implantation,[9] plasma bombardment,[10] and thermal annealing[11] have been made to enhance the field-emission properties of various one-dimensional nanostructures. Over the past decade nanostructures such as carbon nanotubes (CNTs),[12] silicon (Si) NWs,[13] ZnO NWs,[14] as well as nanoheterostructures, such as CNTs grown on Si NWs,[15] ZnO NWs grown on C cloth,[16] and ZnO NWs grown on pyramidlike CNT micropatterns, have been investigated as possible field emitter materials.

Among various ZnO nanostructures, vertically aligned NWs have a variety of application ranging from solar cells,[17] UV lasers,[18] light-emitting diodes,[19] and piezo-nanogenerators,[20] to field-emission devices.[21,22] However, it has been reported that FE properties are mainly dependent on the morphology, dimension, and apex geometry of one-dimensional nanomaterials.[23] Besides external causation, the internal or intrinsic features are also crucial to the FE properties of materials. For practical application in FE and relative area, investigation on intrinsic FE properties of doped ZnO nanomaterials is indispensable. Because of the increasing needs of field-emission devices, in this article, an attempt is made to further improve the FE properties of ZnO NWs by fabricating vertically oriented well aligned ordered arrays of In-doped ZnO NWs and their optical and field-emission properties have been investigated. To the best of our knowledge, no work has been reported to date that is relevant to FE from doped aligned NWs.

2. EXPERIMENTAL SECTION

2.1. Synthesis of In-Doped and Pure ZnO Nanowires. Large scale syntheses of vertically oriented aligned arrays of In-doped ZnO

Received: January 25, 2011
Accepted: March 16, 2011
Published: March 16, 2011

 © 2011 American Chemical Society

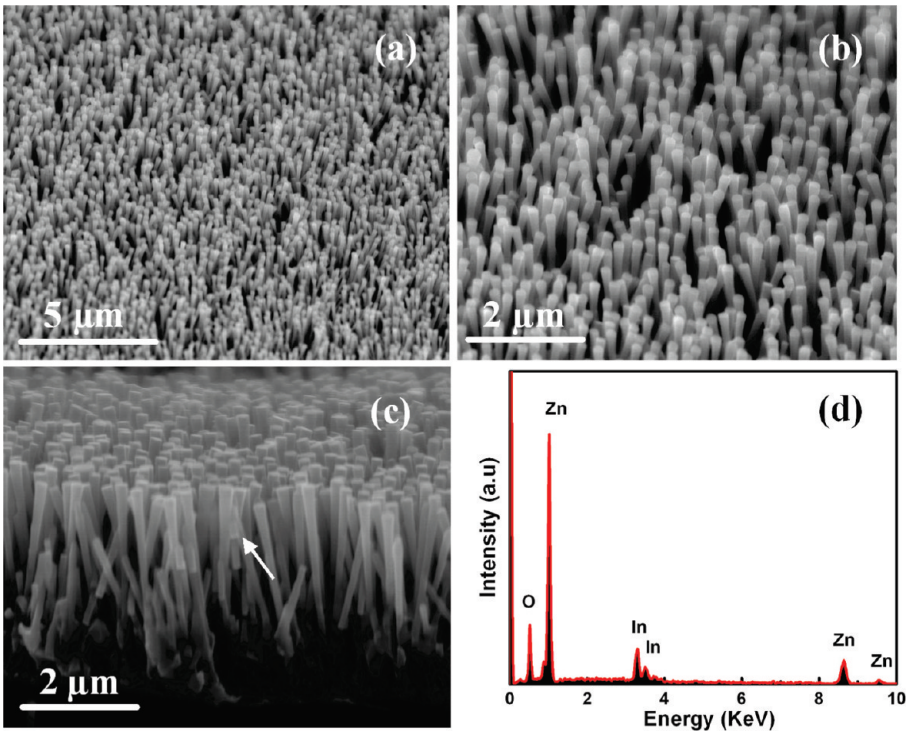

Figure 1. SEM images of the vertically oriented well aligned In-doped ZnO NWs on Zn substrate: (a) low-magnification, (b) high-magnification, (c) cross-sectional view.

NWs was carried out in a horizontal quartz tube furnace via chemical vapor deposition (CVD), where the temperature, pressure and flow rates of working gases are well controlled. In this process, a crucible containing the mixture of Zn, ZnO and In (indium 99.998%, Aldrich) powders with 2:1:1 (weight/mass) ratio, was placed in the central region of the quartz tube furnace. A piece of Zn coated with Au film was placed at the downstream of the tube at about 25 cm away from the source where the temperature about 550 °C. The tube was sealed and evacuated to a pressure of (133.32 Pa). The furnace was then heated to 700 °C at a rate of 20 °C min^{-1} and kept at this temperature for 1 h. A constant flow of high-purity Ar was fed into the tube at a flow rate of 200 sccm throughout the entire heating and cooling processes. Highly pure O_2 was continuously fed into the tube at a flow rate of 3.3 sccm when the furnace temperature was at 700 °C. After the furnace was naturally cooled to room temperature, the white product deposited on the Zn wafer was collected. Pure ZnO NWs was also carried out in the same horizontal quartz tube furnace with the same Zn:ZnO (2:1 weight/mass) ratio under the same experimental conditions.

2.2. Apparatus. The products were characterized by using XRD (TTR-III X-ray Diffractometer), scanning electron microscope (SEM- 6301F), EDS, high resolution TEM (JEM-2011), and XPS (PHI Quantera). PL measurement was conducted at room temperature using the 325 nm line of a He - Cd laser as the excitation source. Field-emission measurement was carried out in a homemade vacuum chamber with a pressure lower than 6×10^{-7} Pa at room temperature under a two-parallel-plate configuration. The samples were connected to the cathode, whereas another parallel stainless-steel plate served as the anode. The distance between cathode and anode was kept about 200, 300, and 400 μm, respectively. A high voltage of ~4 kV was applied before each measurement for the removal of contaminants and degassing the samples. After that a voltage with a sweep step of 50 V was applied between the anode and cathode to supply an electric field *E*. The emission current was monitored by a Keithley 485 picoammeter.

3. RESULTS AND DISCUSSION

3.1. Morphological Characteristics. Figure 1a shows the low-magnification SEM image of the high density uniformly grown vertically oriented well-aligned In-doped ZnO NWs over the entire substrate. It shows that the Au film not only acts as a catalyst but also assist in the uniform growth of NWs. Figure 1b illustrates the high-magnification SEM image and shows the length of NWs is in the range of 3−6 μm and the diameter at the root and tip are in the range of 150 and 300 nm, respectively. Figure 1c presents cross-sectional view SEM image of the as grown In-doped ZnO NWs. The layer appears to be homogeneous and uniform. There is an excellent adherence and connection between In-doped ZnO NWs and Zn substrate. The chemical composition of the doped sample is investigated through EDS as shown in Figure 1d. The spectrum taken from the arrow point in Figure 1c consists of Zn, O, and In peaks and confirms the presence of In content about 2.5% into the product.

3.2. Structural and Compositional Analysis. Figure 2 shows the XRD pattern of the In-doped and pure ZnO samples, in which all the major peaks can be well assigned to those of wurtzite (hexagonal) ZnO with lattice constants of a = 0.325 nm and c = 0.521 nm (JCPDS: 36−1451). The presence of two weak Zn peaks in the pattern reveals that a small amount of Zn powder remains phase separated during the experiment. There is no trace of any crystalline secondary phase which verifies the substitution of In into ZnO lattice. It has been found that the intensity of (002) peak is much stronger than that of other peaks, suggesting the (001) crystal face might be the primary face of the NWs. The inset of Figure 1 shows the comparison of In-doped and undoped NWs in the range 2θ = 31−37° corresponding to (100), (002) and (101) peaks. By monitoring the positions of the peaks, it can be seen that all the peaks shift slightly toward the smaller angle

side. The peaks shift was attributed to the lattice expansion induced by the In-doped. The evaluated *c*-axis lattice constant of the In-doped NWs is 0.5240 ± 0.0005 nm, which is much larger than that of pure ZnO (c = 0.5109 nm). This shows that as the In is introduced into ZnO, some In atoms lodge in the position of Zn atoms. Because the radius of In^{3+} (0.081 nm) is larger than that of Zn^{2+} (0.074 nm), the lattice constant c increases.

TEM is employed to characterize the as-synthesized In-doped ZnO NWs and to investigate the effect of In-doping on its structure. Figure 3a shows the low-magnification TEM image of the In-doped ZnO NW and illustrates that the diameter at the root and top is not homogeneous and vary along the wire length with an average radii about 250 nm. The SAED pattern for each NW is found to be identical to the entire part of the doped NW as shown in Figure 3b. HRTEM image in Figure 3c taken from the rectangular area in Figure 3a demonstrate the high-quality single-crystalline nature of the as-grown doped NWs along a *c*-axis orientation. It is also found that the surface of the NWs has ripplelike edges that are due to the In incorporation. The interplanar distance of fringes is measured to be 0.52 nm, which corresponds to the spacing of the (001) plane. The HRTEM analysis are also consistent with the XRD pattern, in which the intensity of the (002) peak is higher than the other peaks, suggesting that the NWs grow along the [002] direction. Figure 3d shows the in situ EDS spectrum of the doped NW taken from the area indicated by arrow in the Figure 3a. It has been found that each NW contains only Zn, O and In peaks which is consistent with the literature. The statistical analysis over a dozen of NWs demonstrates the uniform composition of In content throughout the specimen. Quantitative analysis reveals that the average amount of In content is about 2.1% in each In-doped NW. The Cu signal comes from the TEM grid used for the measurement.

To further confirm the purity and composition of arrays of In-doped NWs, high resolution XPS analysis has been performed. The XPS spectra of In3d, Zn 3p and O1s are shown in Figure 4. The spectrum in Figure 4a shows two significant binding energy peaks at 444.96 and 452.33 eV corresponding to the electronic states of

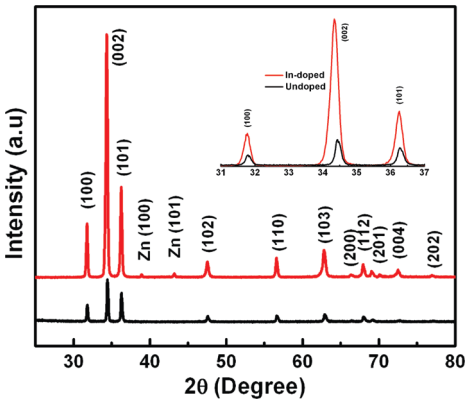

Figure 2. XRD spectra of In-doped and pure ZnO NWs. The inset shows the XRD comparison of both samples in the range $2\theta = 31-37°$.

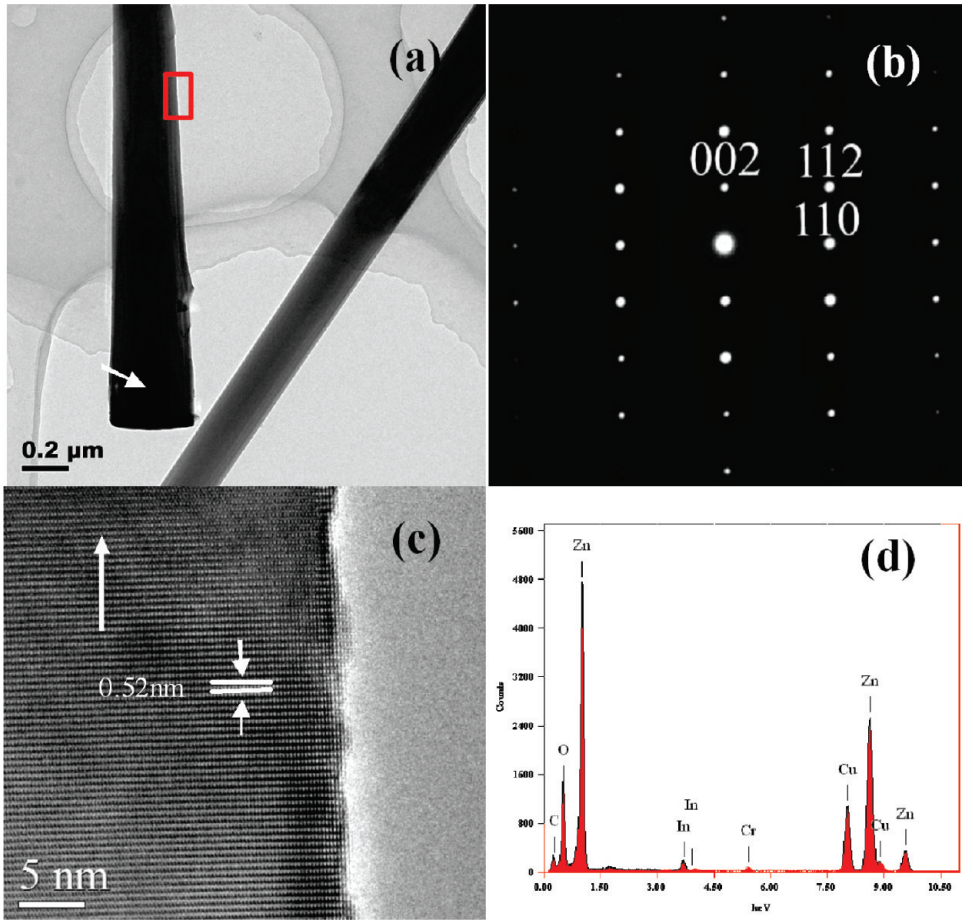

Figure 3. (a) TEM image of the In-doped ZnO NWs, (b) SAED (c) HRTEM image, and (d) corresponding EDS spectrum.

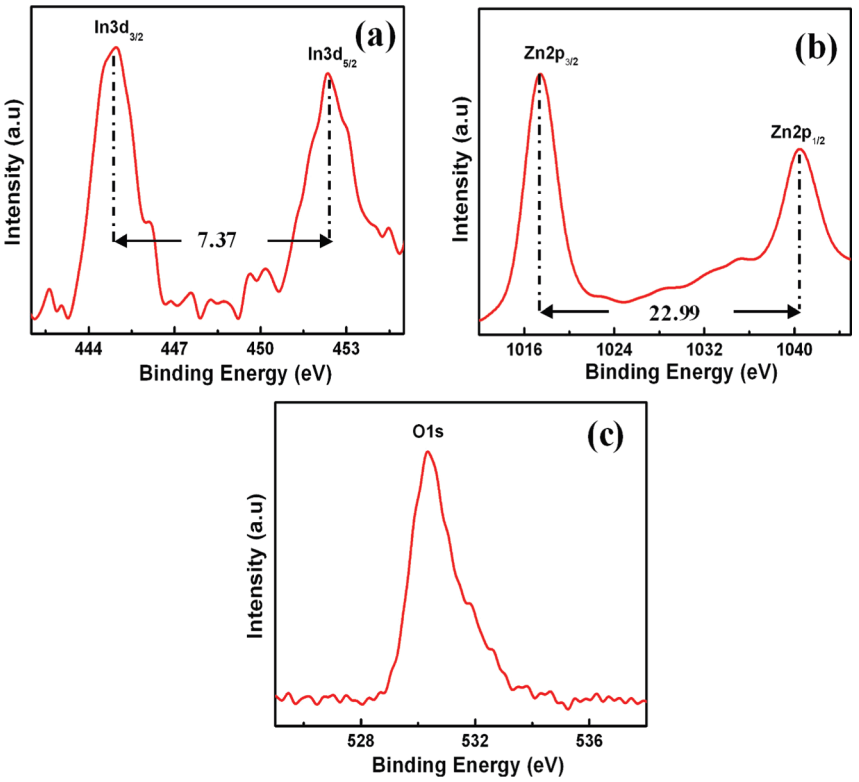

Figure 4. XPS spectra of In-doped ZnO NWs corresponding to (a) In3d3, (b) Zn2p, (c) O1s.

$In3d_{3/2}$ and $In3d_{5/2}$ respectively. Two small satellite peaks are also present along with In3d peaks, which confirm the successful substitution of Indium into ZnO NWs. On the other hand, two peaks at 1017.4 and 1040.39 eV corresponding to $Zn2p_{3/2}$ and $Zn2p_{1/2}$ are shown in Figure 4b. The energy difference between two In3d peaks is 7.37 eV and for Zn2p peaks is 22.99 eV, which agrees well with the standard value of 7.5 and 22.97 eV respectively.[24,25] From the close observation, it is observed that binding energy of In3d peaks exhibit a positive shift in comparison to standard value of In, which is probably caused by electron transfer from ZnO to In due to the strong electronic interaction between In and oxide support. In contrast, the binding energy of Zn2p peaks exhibits a negative shift due to the electronegativity (χ) difference between Zn (χ = 1.65) and In (χ = 1.78). The scan of O1s spectrum is shown in Figure 4c, exhibiting a peak at 530.3 eV which is attributed to oxidized metal ions in the film, viz, O−In and O−Zn, in the ZnO lattice. This implies that In doping can significantly influence the structure of valence band states. Therefore, XPS analysis again confirms the successful incorporation of In into ZnO NWs. Furthermore, the average contents of In are also consistent with the EDS measurements. It has already been found that vertically oriented aligned NWs have great impact on the optical as well as field-emission properties.

3.3. Photoluminescence. It is generally accepted that there are two emission bands in the PL spectrum of ZnO. One is in the UV range, which is associated with exciton emission, and another is in the visible range, which originates from the electron−hole recombination at a deep level, caused by oxygen vacancy or zinc interstitial defects.[26] A comparison of the PL spectra of the In-doped ZnO and that of ZnO NWs is illustrated in Figure 5. A strong UV emission peak 'c' around 381 nm is observed for well aligned In-doped ZnO NWs arrays along with almost negligible

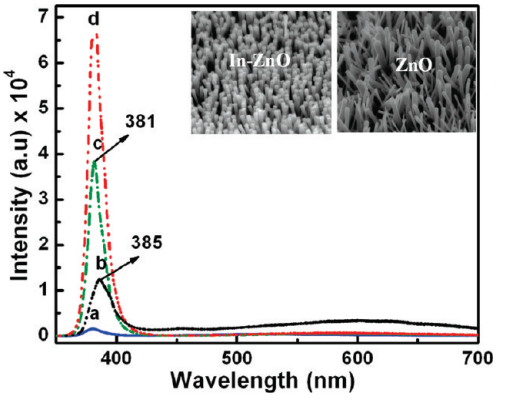

Figure 5. Room-temperature PL spectra of pure "b" and In-doped ZnO NWs obtained at 0.1, 1, and 10 kW/cm^2 laser excitation powers indicated as "a", "c", and "d".

visible emission centered at 540 nm, which indicate the high crystalline quality of In-doped arrays. Besides this, a weak UV emission peak 'b' (385 nm) as well as a broad green band centered at 592 nm occurred for ZnO NWs, which indicates there may be more defects induced during the growth process. In addition, the UV emission peak position of aligned In-doped ZnO NWs shows a blue shift compare with that of ZnO NWs, which is attributed to the shift of the optical band gap in In-doped NWs as reported.[27] Indium dopants contribute more electrons to take up the energy levels located at the bottom of the conduction band. Under excitation with laser at 325 nm, exciton attains energy and move to higher energy levels at the bottom of conduction band. Radiative recombination of these excitons

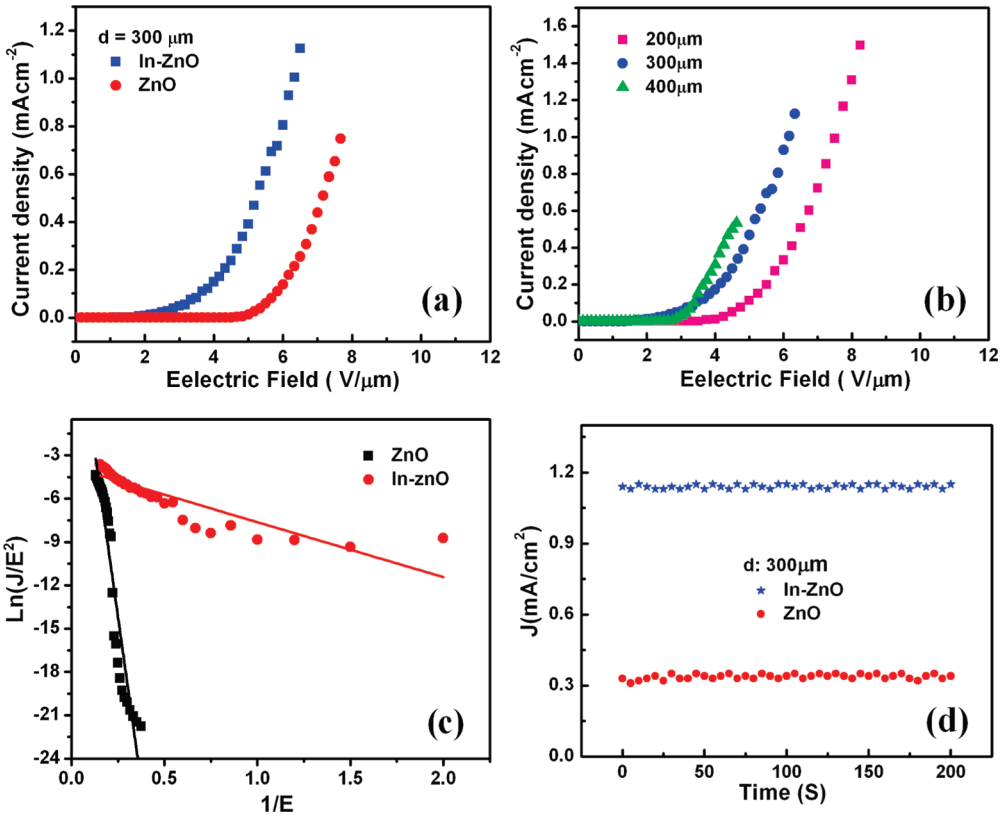

Figure 6. (a) $J-E$ plot comparison of pure and In-doped ZnO NWs at a measuring distance of 300 μm; (b) $J-E$ plots of field emission from well aligned In-doped ZnO NWs at measuring distances of 200, 300, and 400 μm; (c) FN plots of the corresponding $J-E$ curves; (d) emission current density as a function of time demonstrates the field-emission stability.

result a blue shift of the UV peak. The PL spectra of In-doped NWs at low (0.1 kW/cm^2) "a" and high (10 kW/cm^2) "d" excitation power are also recorded as shown in Figure 5. It can be seen that as the excitation power increases, the UV peak intensity also increases, which further proves the excess exciton origin of the UV peak. It has already been proved that the intensity of free exciton emission band grows linearly with the excitation power for bulk ZnO.[28] Therefore, our result agrees with the previous report. The inset shows the SEM images of the two samples.

3.4. Field Emission. The comparison curves of the current density J verses applied electric field E measured at the same condition (d = 300 μm) from well aligned In-doped ZnO NWs and those of pure ZnO NWs are shown in Figure 6a. The turn-on fields, (defined as the E corresponding to the J of 0.01 mA cm^{-2}) of two samples are 2.4 and 4.9 V μm^{-1}, respectively. The threshold fields (defined as the E where J arrives at 0.1 mA cm^{-2}) of In-doped and pure ZnO NWs are 3.5 and 5.6 V μm^{-1} respectively. It is evident that the field-emission properties of the ZnO NWs are considerably improved after In-doping with much lower turn-on and threshold field compared to that of the pure ZnO NWs. From the close observation, it can be clearly observed that the current density has been significantly increased from 0.31 to 1.13 mA cm^{-2} under the same electric field of 5.9 V μm^{-1} for In-doped NWs. Such a significant FE performance of In-doped NWs is attributed due to the In-dopant, because In-dopant provides more electron in the conduction band of NWs as discussed in the PL performance. The FE performance is good in agreement with the PL results.

Figure 6b shows the $J-E$ curves of the aligned In-doped NWs at various measuring distances, 200, 300, and 400 μm between the two electrodes. The sample shows the steady emission current at each distance. Also at each distance the $J-E$ curves have been measured more than 10 times and found to be excellent reproducible.

The emission current−voltage characteristics of both samples are further analyzed by Fowler−Nordheim ($F-N$) equation. According to the FN theory, the relationship between J and E can be described as follows [29]

$$J = A\left(\frac{\beta^2 E^2}{\Phi}\right)\exp\left(\frac{B\Phi^{3/2}}{\beta E}\right)$$

Where A = 1.54 × 10^{-10} (A V^{-2} eV), B = 6.83 × 10^9 (V m^{-1} eV $^{-3/2}$), and Φ is the work function, which is about 5.4 eV for ZnO NWs.[30] B is the field enhancement factor, which reflects the ability of the emitters to enhance the local electric field and can be calculated from the FN plot.

Figure 6c shows the linear dependence of the corresponding $\ln(J/E^2)$ vs E^{-1} (F−N) plots of In-doped and pure ZnO NWs with different slopes, indicating the field emission process from them is a barrier tunneling, quantum mechanical process. According to the F−N theory, the slope of the FN plot is equal to $-B\Phi^{3/2}\beta^{-1}$. The slops obtained from the FN plots can be used to estimate the β value. A number of experiments are performed to ensure the stability and reproducibility. The average value of β is found to be ∼9490 ± 2 for In-doped ZnO NWs. This obtained value is much higher than the values recently reported by other groups as shown in Table 1.

The emission current stability of In-doped and pure ZnO NWs is also tested by measuring current density at 300 μm, under a constant

Table 1. FE Characteristics of Some ZnO Nanostructures Field Emitters Recently Reported in the Literature

ZnO emitter	turn-on field (V μm^{-1})[a]	field enhancement factor (β)	ref
nanoneedles	2.4	1464	31
nanopins	1.92 at 0.1 $\mu A\ cm^{-2}$	657	32
tetrapod-like	1.6 at 1 $\mu A\ cm^{-1}$	6285	33
nanorods arrays	2.98	1732	34
N-doped nanobullet	2.9	1800	35
ZnO on rough -SiRs	2.9	1311	36
tailored nanorods	1.8 at 0.1 $\mu A\ cm^{-2}$	5750	37
urchine-like	3.7	239	38
propeller-like	4.36	1294	39
In-nanorods	4.7	4660	40
N-implantation NWs	2.4 at 0.1 $\mu A\ cm^{-2}$	2100	41
pure NWs	4.9	394	present work
In-doped NWs	2.4	9490	present work

[a] Turn-on field is at current density of 10$\mu A cm^{-2}$.

electric field of 5.9 V μm^{-1} as shown in Figure 6(d). It can be seen that no obvious degradation of FE current density is observed. The emission current fluctuation is about 5 and 8% during the 200 s with keeping constant current density about 1.13 and 0.32 mA cm^{-2} for In-doped and pure ZnO NWs, respectively. These results exhibit the excellent emission stability of the well-aligned In-doped ZnO NWs, which make them highly valuable for practical applications as field emitter. Thus the overall FE performance of In-doped ZnO NWs arrays, such as turn-on and threshold fields, and β factor are all excellent than that of pure ZnO NWs because of the high aspect ratio, good alignment, and In-doping ability. All these factors are very important for a good field emitter.

4. CONCLUSIONS

In summary, successfully synthesized vertically oriented well-aligned In-doped ZnO NWs are found to be single crystals grown along the *c*-axis. The optical property exhibits the tailoring of the band gap with the In dopant. The FE property shows a significant decrease in the turn-on electric field from 4.9 to 2.4 V μm^{-1} after In-doping. Furthermore, an increase in emission current density from 0.31 to 1.13 mA cm^{-2} is achieved under the same electric field of 5.9 V μm^{-1}. The estimated β factor for doped NWs is found to be much higher than that of any previous report. The excellent optical and field-emission behavior of NWs is attributed to the In-doping ability, good alignment, high aspect ratio, and better crystalline quality. This method provides a simple and low-cost approach for the large scale production of nanomaterials with high FE performance to fabricate field emitters such as display panels and light sources.

AUTHOR INFORMATION

Corresponding Author

*E-mail: Jzhu@mail.tsinghua.edu.cn.

ACKNOWLEDGMENT

This work is financially supported by National 973 Project of China and Chinese National Nature Science Foundation. This work made use of the resources of the Beijing National Center for Electron Microscopy. The authors are also grateful to the Higher Education Commission (HEC) Pakistan for the financial support to M.A.

REFERENCES

(1) Ahmad, M.; Zhu, J. *J. Mater. Chem.* **2011**, *21*, 599.
(2) De Heer, W. A.; Chatelain, A.; Ugarte, D. A. *Science* **1995**, *270*, 1179.
(3) Pan, N.; Xue, H.; Yu, M.; Cui, X.; Wang, X.; Hou, J. G.; Huang, J.; Deng, S. Z. *Nanotechnology* **2010**, *21*, 225707.
(4) Yan, X.; Tay, B. K.; Miele, P. *Carbon* **2008**, *46*, 753.
(5) Fancher, C. A.; De Clera, H. L.; Thomas, O. C.; Robinson, O. W.; Bowen, K. H. *J. Chem. Phys.* **1998**, *109*, 8426.
(6) Liao1, L.; Li, J. C.; Wang, D. F.; Liu, C; Liu, C S.; Fu, Q.; Fan, L. X. *Nanotechnology* **2005**, *16*, 985.
(7) Ahmad, M.; Pan, C.; Yan, W.; Zhu, J. *Mater. Sci. Eng., B* **2010**, *174*, 55.
(8) Ahmad, M.; Zhao, J.; Iqbal, J.; Miao, W.; Xie, L.; Mo, R.; Zhu, J. *J. Phys. D: Appl. Phys.* **2009**, *45*, 165406.
(9) Chen, M. Y.; Wu, K. Y.; Hwang, J.; Chang, M. T.; Chou, L. J.; Kou, C. S. *Nanotechnology* **2007**, *18*, 455706.
(10) Zhao, Q.; Cai, T.; Wang, S.; Zhu, R.; Liao, Z.; Yu, D. *Appl. Phys. A: Mater. Sci. Process.* **2010**, *100*, 165.
(11) Zhao, Q.; Feng, S. Q.; Zhu, Y. W.; Xu, X. Y.; Zhang, X. Z.; Song, X. F.; Xu, J.; Chen, L.; Yu, D. P. *Nanotechnology* **2006**, *17*, S351.
(12) Calderón-Colón, X.; Geng, H.; Gao, B.; An, L.; Cao, G.; Zhou, O. *Nanotechnology* **2009**, *20*, 325707.
(13) Tzeng, Y. F.; Wu, H. C.; Sheng, P. S.; Tai, N. H.; Chiu, H. T.; Lee, C. Y.; Lin, I. N. *ACS Appl. Mater. Interfaces* **2010**, *2*, 331.
(14) Chen, C. H.; Chang, S. J.; Chang, S. P.; Tsai, Y. C.; Chen, I. C.; Hsueh, Y. J.; Hsu, C. L. *Chem. Phys. Lett.* **2010**, *490*, 176.
(15) Wu, H. C.; Tsai, T. Y.; Chu, F. H.; Tai, N. H.; Lin, H. N.; Chiu, H. T.; Lee, C. Y. *J. Phys. Chem. C* **2010**, *114*, 130.
(16) Jo, S. H.; Banerjee, D.; Ren, Z. F. *Appl. Phys. Lett.* **2004**, *85*, 1407.
(17) Law, M.; Greene, L. E.; Johnson, J. C.; Saykally, R.; Yang, P. *Nat. Mater.* **2005**, *4*, 455.
(18) Huang, M. H.; Mao, S.; Feick, H.; Yan, H. Q.; Wu, Y. Y.; Kind, H.; Weber, E.; Russo, R.; Yang, P. D. *Science* **2001**, *292*, 1897.
(19) Sun, X. W.; Huang, J. Z.; Wang, J. X.; Xu, Z. *Nano Lett.* **2008**, *8*, 1219.
(20) Qin, Y.; Wang, X.; Wang, Z. L. *Nature* **2008**, *451*, 809.
(21) Li, L.; Fang, X.; Chew, H. G.; Zheng, F.; Liew, T. H.; Xu, X.; Zhang, Y.; Pan, S.; Li, G.; Zhang, L. *Adv. Funct. Mater.* **2008**, *18*, 1080.
(22) She, J.; Xiao, Z.; Yang, Y.; Deng, S.; Chen, J.; Yang, G.; Xu, N. *ACS Nano* **2008**, *2*, 2015.

(23) Huang, Y. H.; Zhang, Y.; Liu, L.; Fan, S. S.; Wei, Y.; He, J. J. *Nanosci. Nanotechnol.* **2006**, *6*, 787.
(24) In *Handbook of X-ray Photoelectron Spectroscopy*; Muilenbenger, G. E., Ed.; Perkin-Elmer Corporation: Eden Prarie, MN, 1979.
(25) Lide, D.R., Ed. *Chemical Rubber Company Handbook of Chemistry and Physics*; CRC Press: Boca Raton, FL, 81st ed., 2000.
(26) Zeng, H. B.; Cai, W. P.; Hu, J. L.; Duan, G. T.; Liu, P. S.; Li, Y. *Appl. Phys. Lett.* **2006**, *88*, 171910.
(27) Chen, Y. W.; Liu, C. Y.; Lu, S. X.; Xu, C. S.; Shao, C. L.; Wang, C.; Zhang, J. Y.; Lu, Y. M.; Shen, D. Z.; Fan, X. W. *J. Chem. Phys.* **2005**, *123*, 134701.
(28) Guo, B.; Qiu, Z. R.; Wong, K. S. *Appl. Phys. Lett.* **2003**, *82*, 2290.
(29) Fowler, R. H.; Nordheim, L. W. *Proc. R. Soc. London, Ser. A* **1928**, *119*, 173.
(30) Jo, S. H.; Banerjee, D.; Ren, Z. F. *Appl. Phys. Lett.* **2004**, *85*, 1407.
(31) Zhao, Q.; Zhang, H. Z.; Zhu, Y. W.; Feng, S. Q.; Sun, X. C.; Xu, J.; Yua, D. P. *Appl. Phys. Lett.* **2005**, *86*, 203115.
(32) Xu, C. X.; Suna, X. W. *Appl. Phys. Lett.* **2003**, *83*, 3806.
(33) Wana, Q.; Yu, K.; Wang, T. H.; Lin, C. L. *Appl. Phys. Lett.* **2003**, *83*, 2253.
(34) Lee, J. H.; Chung, Y. W.; Hon, M. H.; Leu, I. C. *Appl. Phys. A: Mater. Sci. Process.* **2009**, *97*, 403.
(35) Gautam, U. K.; Panchakarla, L. S.; Dierre, B.; Fang, X.; Bando, Y.; Sekiguchi, T.; Govindaraj, A.; Golberg, D.; Rao, C. N. R. *Adv. Funct. Mater.* **2009**, *19*, 131.
(36) Wu, H. C.; Tsai, T. Y.; Chu, F. H.; Tai, N. H.; Lin, H. N.; Chiu, H. T.; Lee, C. Y. *J. Phys. Chem. C* **2010**, *114*, 130.
(37) Zeng, H.; Xu, X.; Bando, Y.; Gautam, U. K.; Zhai, T.; Fang, X.; Liu, B.; Golberg, D. *Adv. Funct. Mater.* **2009**, *19*, 3165.
(38) Jiang, H.; Hu, J. Q.; Gu, F.; Li, C. S. *Nanotechnology* **2009**, *20*, 055706.
(39) Yan, H. L.; Wan, J. B.; Zhong, X. L. *J. Mater. Sci.: Mater. Electron.*, DOI 10.1007/s10854-010-0200-1
(40) Fang, T. H.; Kang, S. H. *Curr. Appl. Phys.* **2010**, *10*, 1076.
(41) Zhao, Q.; Gao, J.; Zhu, Rui.; Cai, T.; Wang, S.; Song, X.; Liao, Z.; Chen, X.; Yu, D. *Nanotechnology* **2010**, *21*, 095701.